

21 Debris Flows and Related Phenomena

C. Ancey

Cemagref, unité Erosion Torrentielle, Neige et Avalanches, Domaine Universitaire, 38402 Saint-Martin-d'Hères Cedex, France

21.1 Introduction

Torrential floods are a major natural hazard, claiming thousands of lives and millions of dollars in lost property each year in almost all mountain areas on the Earth. After a catastrophic eruption of Mount St. Helen in the USA in May 1980, water from melting snow, torrential rains from the eruption cloud, and water displaced from Spirit Lake mixed with deposited ash and debris to produce very large debris flows and cause extensive damage and loss of life [1]. During the 1985 eruption of Nevado del Ruiz in Colombia, more than 20,000 people perished when a large debris flow triggered by the rapid melting of snow and ice at the volcano summit, swept through the town of Armero [2]. In 1991, the eruption of Pinatubo volcano in the Philippines disperses more than 5 cubic kilometres of volcanic ash into surrounding valleys. Much of that sediment has subsequently been mobilised as debris flows by typhoon rains and has devastated more than 300 square kilometres of agricultural land. Even, in European countries, recent events that torrential floods may have very destructive effects (Sarno and Quindici in southern Italy in May 1998, where approximately 200 people were killed).

The catastrophic character of these floods in mountainous watersheds is a consequence of significant transport of materials associated with water flows. Two limiting flow regimes can be distinguished. *Bed load* and *suspension* refer to dilute transport of sediments within water. This means that water is the main agent in the flow dynamics and that the particle concentration does not exceed a few percent. Such flows are typically two-phase flows. In contrast, *debris flows* are mass movements of concentrated slurries of water, fine solids, rocks and boulders. As a first approximation, debris flows can be treated as one-phase flows and their flow properties can be studied using classical rheological methods. The study of debris flows is a very exciting albeit immature science, made up of disparate elements borrowed from geomorphology, geology, hydrology, soil mechanics, and fluid mechanics. The purpose of this chapter is to provide an introduction to physical aspects of debris flows, with specific attention directed to their rheological features. Despite attempts to provide a coherent view on the topic, coverage is incomplete and the reader is referred to a series of papers and books. Three books are particularly commendable [3,4,5]. Some review papers provide interesting overviews, introducing the newcomers to the field to the main concepts [6,7,8]. The background material in rheology can be found in Chaps. 2 and 3.

21.2 A Typology of Torrential Flows

21.2.1 The Watershed as a Complex Physical System

The notion of torrent refers to a steep stream, typically in a mountainous context. According to a few authors, a stream can be referred to as a *torrent* as soon as its mean slope exceeds 6%. For bed slopes ranging from 1% to 6%, it is called a *torrential river*. For bed slopes lower than 1%, it can be merely called a *river*. In addition to the slope, the sediment supply is generally considered as another key ingredient in torrential watersheds. Depending on the nature of the soil and relief, slopes can provide a large quantity of poorly sorted solid materials to torrents. Supplied materials have sizes ranging typically from 1 μm to 10 m. The situation is very different from the one encountered for streams on a plain, where bed material is much finer and sorted (typically 1 μm to 10 cm) since it generally results from transport that occurred during previous floods. Finally, one of the chief ingredients of torrential watersheds is water. Due to the small dimensions of torrential watersheds (typically from 0.1 km^2 to 100 km^2) and the steep slopes, floods are sudden, short, and violent. The flood regime differs significantly from plain floods, which are characterised by slower kinetics and smoother variations with time. Figure 21.1 depicts a typical watershed. The upper part is generally degraded and submitted to erosion to a more or less large extent. It supplies water and sediment to the floods. Below this basin, the torrent enters a gorge, sometimes with very abrupt flanks depending on the nature of the soil. Then the torrent discharges onto the alluvial fan. The slope transition between the gorge and the alluvial provides interesting information on bed equilibrium. Generally, a watershed with an abundant supply of sediment and intense bed load transport in the past is characterised by a smooth transition from channel to fan.

For plain rivers, sediment transport results from the action of water: water entrains materials either by pushing them along the bed (bed load transport) or by keeping them in suspension as a result of turbulence (suspension). In a torrential context, as soon as the bed inclination is sufficiently high, gravity has a more pronounced role on sediment transport. Therefore, on the one hand, bed load transport is more intense and on the other hand, a new mode of transport arises: debris flow. We can define them as follows:

- *Debris flows* are highly concentrated mixtures of sediments and water, flowing as a single-phase system. Debris flows look like mudslides and landslides except that their velocity and the distances they travel are much larger. It is worth noticing that in the literature there are many terms used to refer to slides and/or debris flows, which is a source of confusion.
- *Bed load transport* involves transportation of sediment by water. Coarse particles (sand, gravel, and boulders) roll and slide in a thin layer near the bed (called the bed layer). Generally fine particles (silts and clays) are brought into suspension as a result of water turbulence. The system is typically made up of two distinct phases: liquid phase (i.e. water) and dispersed (solid) phase.

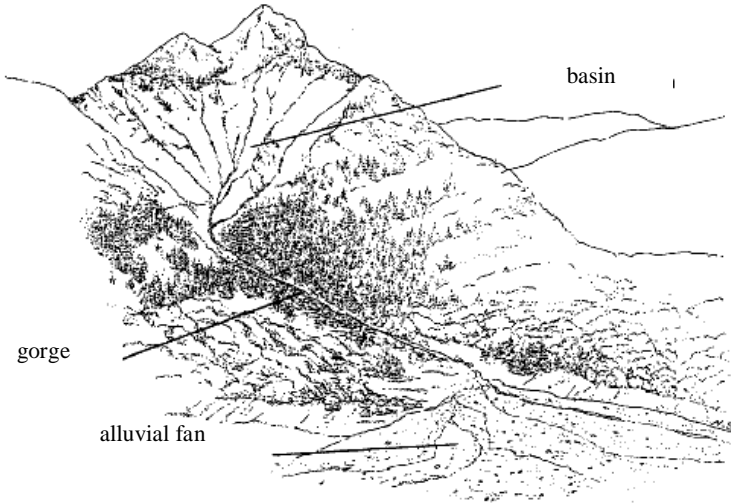


Fig. 21.1. A typical watershed (courtesy of Nicole Sardat)

21.2.2 Types of Transport

In the laboratory, it is possible to simulate torrential phenomena using an inclined channel with a mobile bed made up of sand and gravel. Figures 21.2 and 21.3 show two very different situations that can be observed when the channel slope is increased by only a few percent. Figure 21.2 corresponds to a slope of 17%. At high discharges, fine particles are in suspension while the coarsest particles are pushed down to the bed. In this photograph the largest particles are stationary and significantly affect water flow. The two phases (solid and liquid) are well separated and water flows much faster than solid particles. When the inclination exceeds a critical value (approximately 20%), significant sudden changes can be observed: a transition from a two-phase flow to a single-phase flow occurs very quickly. The mixture takes on the appearance of a “viscous” homogeneous fluid flowing down the bed. Figure 21.3 (slope of 27%) illustrates such a transition and the resulting mass movement. Most laboratory experiments conducted with water flows on erodible beds have shown that the bed inclination θ is a key factor in sediment transport dynamics [9,10,11,12,13]. On the whole it has been observed that:

- $\theta < 20\%$: at sufficiently high water discharges, water flow induces intense bed load transport near the bed. As a first approximation, the water and solid discharges (respectively q_w and q_s) are linearly linked: $q_s \approx 8.2\theta^2 q_w$ (this relationship is an overly simplified expression of discharge obtained by Smart and Jaeggi [11] or Rickenmann [10]). Three layers can be distinguished: the bed made up of stationary particles (that can be eroded), the (active) bed layer in which sediment of all sizes is set in motion (rolling and sliding), and the water layer, where fine particles are in suspension or in saltation. In two-

phase flows of this type the solid concentration (ratio of solid volume to total volume) does not exceed 30%.

- $\theta > 20\%$: at sufficiently high water discharges, bed load transport is unstable. It changes into a dense single-phase flow. The solid concentration is very high, ranging from 50% to 90% depending on the size distribution of particles. Such flows simulated in the laboratory correspond to debris flows in the field.



Fig. 21.2. Small-scale simulation of bed load transport in the laboratory. The solid and liquid phases are distinct (water was coloured with fluoresceine). The typical flow depth in these experiments was 1 cm

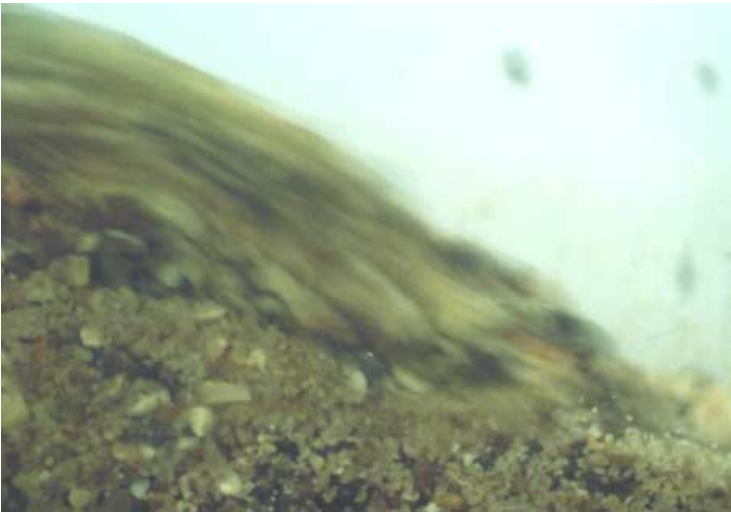


Fig. 21.3. Small-scale simulation of a debris flow in the laboratory. The solid and liquid phases are mixed

In the laboratory, the transition from bed load transport to debris flow is reflected by a discontinuity in the solid concentration. It is suspected that such a discontinuity still exists in the field, at least in the Alps, but the underlying mechanisms are unknown. It is worth noticing that in the field, debris flows can also form from landslides [7]. In this case, the transformation mechanisms are similar to soil liquefaction processes (rapid creep of saturated soils). In the following, we will tackle the problem of debris flows, which are intrinsic to mountain torrents and steep slopes. Other chapters in this book deal with bed load transport.

21.3 Initiation, Motion, Effects of Debris Flow

21.3.1 Initiation

The torrential activity of a watershed depends on many parameters. Debris flows are common in some areas and uncommon in others. In areas prone to debris flow formation, their frequency also varies. In some watersheds, several debris flows occur each year while for other torrents, they are rare. Conditions for initiation of most debris flows usually include:

- *Steep slopes.* In the Alps, slopes in excess of 70% are liable to surface erosion (sediment transport induced by runoff) and landslides (soil failure leading to large masses of saturated materials coming loose).
- *Abundant supply of unconsolidated materials.* Debris flows originate either from the simultaneous contributions of many material sources or from a single source (landslides):
 - Slow and continuous erosive processes on slopes in the drainage basin form deposits of materials in the torrent bed. Such deposits can be subsequently mobilised during intense floods and then transform into debris flows. In this case, debris flow originate as a slurry, primarily of water and fine particles, which erodes its channel and grows in size. Presumably instabilities in the bed load transport (such as those observed in the laboratory) arise and enable debris flow initiation. Usually the volume produced every year by erosion over the whole drainage basin is small and thus the amount of sediments that can be involved by a single debris flow is limited ($< 10^5 \text{ m}^3$). In the field, the absence of failure surfaces and the presence of rills in the drainage basin are generally evidence that a debris flow has picked up coarse materials from the bed.
 - Old ill-consolidated deposits (moraines, massive rockfall deposit, etc.) can mobilise into landslides to form debris flows. In this case, the volume of materials involved can be very large ($> 10^5 \text{ m}^3$) depending on the total volume made available by the source. Likewise, certain soils (e.g. gypsum) are very liable to landslides and can supply materials to debris flows. Presumably, initiation is due to a combination of several mechanisms: rapid creep deformation, increase in pore pressure, increase in load, erosion at the foot of

the landsliding mass, etc. In the field, the presence of a failure surface can clearly serve to identify the source of material.

- *Large source of moisture.* Most of debris flows occur during or after heavy and sustained rainfalls. In some cases, snowmelt can be sufficient to form debris flows. (There are many other ways in which water can be provided for the formation of debris flows: thawing soil, sudden drainage of lakes, dam break, etc., but these are much less frequent.) A high liquid water content seems to be a necessary condition for the soil to be saturated, which cause: intense surface runoff, and an increase in the pore-water pressure (presumably leading to Coulomb slope failure).
- *Sparse vegetation.* Vegetation plays a role by intercepting rainfall (limitation of runoff) and increasing soil cohesion (root anchorage). Vegetation reduces the initiation potential to a certain extent but does not completely inhibit formation of debris flows. Many observations have shown that debris flows also occur in forested areas.

21.3.2 Motion

On the whole, debris flows are typically characterised by three phases, that can change with time (see Fig. 21.4):

- At the leading edge, a granular front or snout contains the largest concentration of big rocks. Boulders seem to be pushed and rolled by the body of the debris flow. The front is usually higher than the rest of the flow. In some cases no front is observed because either it has been overtaken by the body (very frequent when the debris flow spreads onto the alluvial fan), or the materials are well sorted and no significant variation in the bulk composition can be detected.
- Behind the front, the body has the appearance of a more fluid flow of a rock and mud mixture. Usually, the debris flow body is not in a steady state but presents unsteady surges. It can transport blocks of any size. Many authors have reported that boulders of relatively small size seem to float at the free surface while blocks of a few meters in size move merely by being overturned by the debris flow. The morphological characteristics of the debris flow are diverse depending on debris characteristics (size distribution, concentration, mineralogy) and channel geometry (slope, shape, sinuosity, width). Debris flows velocity varies very widely but, on the whole, ranges from 1 m/s to 10 m/s [14]. The fastest debris flows are reported to move at more than 20 m/s [14]. Flowing debris can resemble wet concrete, dirty water, or granular material but whatever the debris characteristics and appearance, viscosity is much higher than for water. Most of the time, debris flows move in a completely laminar fashion, but they can also display minor turbulence (or be highly turbulent).
- In the tail, the solid concentration decreases significantly and the flow looks like a turbulent muddy water flow.

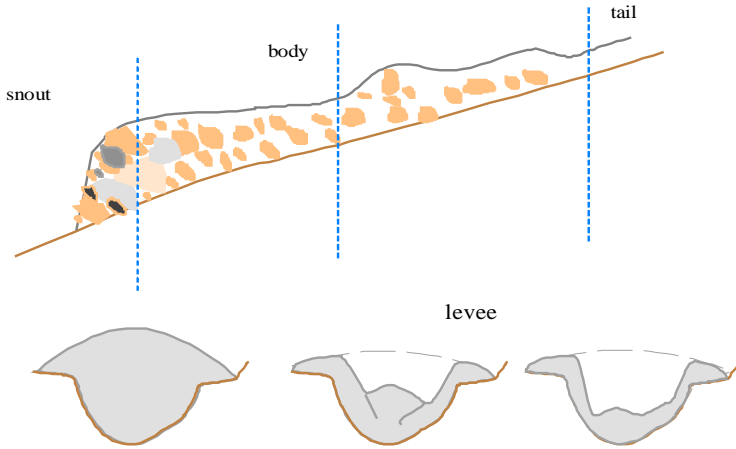


Fig. 21.4. Idealised representations of a debris flow (longitudinal profile and cross section). The different sections correspond to the dashed lines of the upper panel. Adapted from [15]

21.3.3 Deposition and Effects

The distance that a debris flow can travel depends a great deal on the mechanical characteristics of the debris as well as the total volume, channel geometry and bed inclination. For instance it is generally observed that a debris flow moving over a flat tilted plane thins by spreading laterally and stops suddenly, seemingly when the thickness reaches a critical value. In contrast, if the debris flow is channelized, it may travel quite a long distance over gentle slopes. In European alpine countries, debris flows (of sufficient volume) generally begin to decelerate when the slope ranges from 10% to 25%. For some torrents, (e.g. Illgraben in Switzerland and Boscodon in France), debris flows can propagate over gentle slopes (of less than 5%). In volcanic soil areas, it has been also demonstrated that lahars (debris flows involving water–ash mixtures) can propagate over very slight slopes (less than 1%) [14].

For some debris flows, constant deposition occurs all along the channel and forms levees on the lateral boundaries of the torrent. Depending on the size distribution of the materials involved in the debris flow, a levee can have various shapes. In most cases, the cross section reveals a curved profile and, when the deposit is dry, it is characterised by strong cohesion. In other cases, the cross section has a straight free surface and even when it is dry, the deposit displays minor cohesion and looks like a sand or gravel heap. Formation of levees is not systematic. Many observers have noticed that, after a debris flow has passed through a channel, the channel bottom and sides have been swept clean of debris.

The alluvial fan is the preferential area for debris-flow deposition owing to the decrease in bed slope and widening of the channel. The slope decrease usually leads to the sudden stopping of the granular front and increase in the flow depth

for the body. In many cases, debris flows overflow the channel banks and spread as broad lobes on the alluvial fan. As for levees, the morphological features of lobes vary widely. For instance, the longitudinal profile of a lobe margin can be curved (parabola-shaped), straight and tilted, or step-shaped. In the latter case, the deposit looks like an alluvial deposit. Although they move at low velocities on the alluvial fan, debris flows can impact or bury structures.

21.4 Debris Flow Classification

The diversity in the morphological features of debris flows provides evidence of different families with specific bulk behaviour. Several classifications have been proposed in the last few years. To date, there is no agreement on the chief characteristics on which classification should rely. Therefore, some classifications are based on the size distribution of materials involved, others only consider the mode of release, etc. Here we are mainly interested in the manner in which a debris flow propagates and therefore we suggest using a classification based on bulk mechanical behaviour. We shall therefore consider three families:

- *Muddy debris flow.* The transported material is usually characterised by a wide particle-size distribution. It is sufficiently rich in clay-like materials for the matrix to have a muddy consistency and lubricate contact between coarse particles. Most of the time, bulk behaviour is typically viscoplastic. That means that the material exhibits both plastic and viscous properties [3,16,17,18,19,20]. When the stress level is low, the material behaves as a solid body, but when the stress level exceeds a critical value (yield stress), it flows as a fluid does. This yield stress confers specific properties to the material. For instance, when a given volume of material is released and spreads down a tilted flat plane, the flow depth decreases regularly. When the flow depth reaches a critical value (depending on the yield stress and the plane inclination), the driving shear stress is lower than the yield stress and the flow stops abruptly. In most cases, the yield stress ranges from 0.5 kPa to 15 kPa. Muddy debris flows can usually propagate over slopes greater than 5%. The limits of deposits are sharp and well delineated. Boulders and gravel are randomly distributed in a finer-grained cohesive matrix. Muddy debris flows are very frequent in the Alps.
- *Granular debris flow.* Although the size distribution is wide, the material is poor in fine (clay-like) particles. Bulk behaviour is expected to be frictional-collisional [23,24,25,26]: it is mainly governed by collisions and friction between coarse particles. Energy dissipation is usually much larger for granular debris flows than for muddy debris flows and thus, granular debris flows require steep slopes (> 15%) to flow. Presumably, as for very large rockfalls, a granular debris flow involving a very large amount of materials may travel large distances over more gentle slopes. In the field, deposits are easily recognised by the irregular chaotic surface. Deposits are generally graded, with coarser debris forming mass deposits and finer debris transported downstream (due to drainage).

- *Lahar-like debris flow.* The particle-size distribution is narrow and the material contains only a small proportion of clay-like materials. This type of debris flow is typical of volcanic soil areas (soils made up of fine ash), but it can be observed on other terrain (e.g. gypsum, loess) [21]. Bulk behaviour is expected to be frictional/viscous: at low shear velocities, particles are in sustained frictional contact and bulk behaviour may be described using a Coulomb frictional equation. At high shear velocity, due to dilatancy and increased fluid inertia, contacts between coarse grains are lubricated by the interstitial fluid [27]. In the laboratory, such materials exhibit very surprising properties: at rest, they look like fine soil (silts) but once they have been stirred up, they liquefy suddenly and can flow nearly as Newtonian fluids. Contrary to muddy debris flows, the yield stress is low and therefore, lahars can move over gentle slopes of less than 1%. Deposits are very thin and flat and look like alluvial deposits.

21.5 Modelling Debris Flows

There are many similarities between debris flows and flowing avalanches. Both are rapid gravity-driven flows of dense materials down mountain slopes. Thus, approaches similar to those developed for modelling avalanches have been proposed (see Chap. 13).

21.5.1 Statistical Approach

A few authors have attempted to relate the runout distance (and other debris flow characteristics) to the watershed features. Extensive work performed by Swiss scientists and engineers has led to different equations [5,28,29]. For instance, using regression analysis, Zimmermann and co-workers found that the most significant variable in the runout distance was the surface of the watershed S (in km^2) [5]: $\alpha = 0.2 S^{-0.26}$, where α is the angle between the line joining the top of the starting zone to the stopping point with respect to the horizontal. Such an equation differs from the ones inferred for avalanches. Indeed, in this latter case, it has been found that the angle α mainly depends on the angle β corresponding to a path characteristic (see Chap. 13). This might mean that, contrary to avalanches, the runout distance of debris flows is less influenced by channel geometry and probably depends a great deal on the sediment volume. Indeed, in the above equation, the watershed-surface dependence does reflect a debris-flow volume dependence since most of the time debris involved in debris flows result from erosion of the drainage basin, thus it is expected to depend on S . The correlation existing between the runout distance and the debris-flow volume has been further demonstrated by Rickenmann [28]. Using data from 82 events, Rickenmann inferred the following statistical equation: $L = 350 V^{0.25}$, where L is the maximum distance (in m) that a debris flow of volume V (in m^3) can travel. Likewise, he found that for a muddy debris flow, the peak discharge Q_p (in m^3/s) can be estimated at: $Q_p = 0.0225 V^{0.8}$, while Mizuyama found that, for a granular debris flow, it can be estimated at: $Q_p = 0.135 V^{0.78}$. It

should be noted that the peak discharge is much higher for granular debris flows than for muddy debris flows.

21.5.2 Deterministic Approach

The distinctions in the spatial scale and model complexity that have been put forward for avalanches, are still valid here. As for avalanches, Voellmy’s model and depth-averaged mass and momentum equations have been proposed.

Empirical Model: The PCM Model Adapted to Debris Flow

Zimmermann has adapted the Perla–Cheng–McClung avalanche-dynamics model to compute characteristics of debris flow [5]. He assumed that a debris flow can be approximated by the motion of a solid block of mass M , subject to a frictional force including two contributions:

- a Coulombic frictional contribution (ground/debris flow): $F_C = \mu M g \cos \theta$,
- a dynamic drag: $F_D = D v^2$,

where μ and D are two parameters, θ is the bed slope. The momentum equation in the downstream direction can then be expressed as follows:

$$\frac{1}{2} \frac{dv}{dx} = g(\sin \theta - \mu \cos \theta) - \frac{D}{M} v^2 . \tag{21.1}$$

Debris flow terrain is represented by a centreline profile stretching from the top of the starting zone to the end of the runout zone. The profile must be subdivided into several segments, which are sufficiently short for the slope to be considered constant. The length of segment i is L_i . At the end of the i^{th} segment, the velocity (v_i^f) depends on the initial velocity (v_i^d) at the top of this segment:

$$v_i^f = \sqrt{a \frac{M}{D} (1 - e^\beta) + (v_i^d)^2 e^\beta} , \tag{21.2}$$

where we have introduced $a = g(\sin \theta - \mu \cos \theta)$ and $\beta = -2L_i/(M/D)$. If the debris flow stops within segment i , then the runout distance (from the beginning of the i^{th} segment) is given by:

$$x_s = \frac{1}{2} \frac{M}{D} \ln \left(1 - \frac{(v_i^d)^2}{aM/D} \right) . \tag{21.3}$$

Velocity at the bottom of a segment, v_i^f , is used to compute velocity, v_{i+1}^d , at the top of the next segment:

$$v_{i+1}^d = \cos(\theta_i - \theta_{i+1}) v_i^f . \tag{21.4}$$

This computation is repeated downslope until the block stops. The values of the two parameters μ and D have been adjusted to 49 events that occurred in

the Swiss Alps. Although this sample size may be considered too small to draw reliable correlations, it can provide helpful trends: μ and D are independent of the volume V and μ depends on the watershed surface. According to Zimmermann and co-workers [5], this dependence might suggest that the runoff over the drainage basin affects the solid concentration, and the frictional coefficient μ . They proposed two correlations:

- Lower value: $\mu = 0.18 S^{-0.30}$.
- Upper value: $\mu = 0.13 S^{-0.35}$.
- The mass-to-drag ratio M/D depends a great deal on size distribution. They found:
 - fine material (clays, fewer blocks): $20 \geq M/D \geq 60$ (average: 40),
 - fine-grained and coarse materials (clays, boulders): $80 \geq M/D \geq 180$ (average: 130),
 - granular materials (sand and gravel): $40 \geq M/D \geq 100$ (average: 70).
- No channelling effect was observed.
- No influence of the starting type (single or multiple sources) was detected regarding the friction coefficients.

Depth-averaged Models

The principles of depth-averaged models have been specified in Chaps. 13 and 22. The chief approximation is to consider the material involved in a debris flow as a homogeneous fluid. Thereby its behaviour can be described using a constitutive equation. Unlike snow, many experiments on debris have been conducted to gain insight into the rheology of these materials [3,20]. In a steady state, the shear stress may be written as follows:

$$\tau = f(\dot{\gamma}, \zeta), \quad (21.5)$$

where τ denotes the shear stress, $\dot{\gamma}$ is the shear rate, and ζ refers to a group of mechanical parameters on which bulk behaviour depends (for instance, this group can include the solid concentration ϕ or other parameters pertaining to the microstructure). Depending on the kind of debris flows, several constitutive equations have been proposed to describe debris flows (cf. also Chaps. 3, 4, 7 and 22):

- For lahar-like debris flows, bulk behaviour may be described using a Newtonian constitutive equation as a first approximation: $\tau = \mu(\phi)\dot{\gamma}$. Viscosity is usually very high, with typical values close to 10^3 Pa s [21].
- For muddy debris flows, bulk behaviour is usually best described using a Bingham or Herschel–Bulkley model: $\tau = \tau_c(\phi) + K(\phi)\dot{\gamma}^n$, where τ_c is the yield stress, K a parameter, n a shear-thinning index ($n \leq 1$, $n = 1$ corresponding to the Bingham model). For a flow to occur ($\dot{\gamma} > 0$), the shear stress must exceed the yield stress τ_c . In the Alps, bulk yield stress values range from 0.5 kPa to 15 kPa and the ratio τ_c/K lies usually in the range 3–10 [22].

- For granular debris flows, bulk behaviour is expected to be frictional and/or collisional. To date there is no unanimity concerning the constitutive equation suitable to describe frictional–collisional flows. Different models have been proposed with very different stress generation mechanisms: collisional Bagnold models [23], collisional kinetic models [26], collisional–frictional constitutive equations [24], models based on pore-pressure effects [7], etc. Further developments on granular flows down steep slopes can be found in Chap. 4.

Once the constitutive equation has been determined, it is possible to compute some characteristics, notably the ones related to a steady state flow. Indeed, the stress distributions are known for steady uniform flows independently of the constitutive equation (cf. Chap. 3). For instance, the shear stress distribution is given by the following equation: $\tau = \rho g(h - y) \sin \theta$, where ρ is the bulk density and $(h - y)$ is the depth with respect to the free surface. Comparing this expression to (21.5) and after integration, we can deduce the velocity field. Further integration leads to the discharge equation. For instance, in the case of a Herschel–Bulkley fluid, we obtain:

$$y \leq h_c \Rightarrow u(y) = \frac{1}{p} \sqrt[n]{\frac{\rho g \sin \theta}{K}} [h_c^p - (h_c - y)^p] , \tag{21.6}$$

$$y \geq h_c \Rightarrow u(y) = \frac{1}{p} \sqrt[n]{\frac{\rho g \sin \theta}{K}} h_c^p , \tag{21.7}$$

where we introduce: $p = 1/n + 1$ and $h_c = h - \tau_c/(\rho g \sin \theta)$. Near the free surface, a non-sheared zone (“plug flow”), characterised by a constant velocity, is observed. An expression of this sort is meaningful provided that the flow depth exceeds a critical value: $h > \tau_c/(\rho g \sin \theta)$. Thus the existence of a yield stress implies the existence of a critical flow depth, under which no steady uniform flow is possible and the existence of critical slope $\sin \theta_c = \tau_c/(\rho gh)$. After integration, the discharge is found to be:

$$q = \frac{1}{p} \sqrt[n]{\frac{\rho g \sin \theta}{K}} h_c^p \left(h - \frac{1}{p+1} h_c \right) . \tag{21.8}$$

The discharge is a strongly non-linear function of the flow depth. As $n \approx 0.3$, this means that small changes in the flow depth can cause large variations in the flow rate. All these computations can be extended to gradually varying flows (i.e. slightly non-uniform and unsteady). In the case of a Herschel–Bulkley fluid flowing down an inclined infinite plane, the resulting motion equation set is (see Chap. 22 for a more complete introduction):

$$\frac{\partial h}{\partial t} + \frac{\partial h \bar{u}}{\partial x} = 0 , \tag{21.9}$$

$$\frac{\partial h \bar{u}}{\partial t} + \frac{\partial h \bar{u}^2}{\partial x} = g \sin \theta - \frac{\tau_p}{\rho} - gh \cos \theta \frac{\partial h}{\partial x} , \tag{21.10}$$

where τ_p is the bottom shear stress:

$$\tau_p = K \left(\frac{1+p}{p} \right)^n \frac{\bar{u}^n}{h_c^{n+1} [(1+p)h - h_c]^n} . \tag{21.11}$$

Generally the motion equation set must be solved numerically since there is no analytical solution apart from the one shown for the steady-state regime. For instance, this can be done using finite-volume numerical models developed for solving hyperbolic differential equations [30,31]. They are now used in engineering problems when accurate results on a complex topography are needed. Approximate analytical or quasi-analytical solutions have also been proposed, notably by Hunt [32,33] and more recently by Huang and Garcia [35,34]. But, compared to experimental data (see Fig. 21.5), such approximations provide correct results at large times (when the flow fairly achieves a steady uniform regime) but fail to capture the flow features at any time. On explanation for partial agreement is that these models neglect the influence of normal stresses [36].

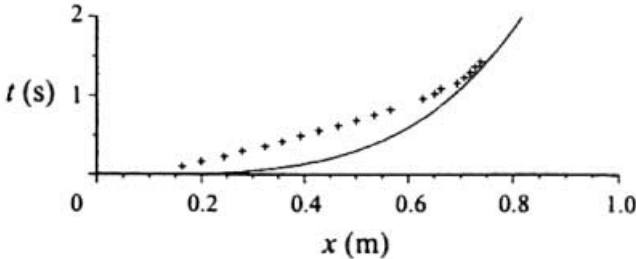


Fig. 21.5. Comparison of computed and measured position of the leading edge of a mud flow. Experiments were carried out in a tank tilted at 11° with kaolinite suspensions (solid concentration $\phi_k = 13.05\%$, released volume 24.7 cm^2). Adapted from [34]. (Courtesy of M.H. Garcia)

In addition to providing the flow characteristics for gradually varied flows, the motion equation set may be used to investigate other interesting properties. For instance, Coussot used a depth-averaged model to demonstrate that free surface flows of Herschel–Bulkley fluids are unstable when the Froude number $Fr = \bar{u}/\sqrt{gh \cos \theta}$ exceeds a critical value (approximately 0.1 in the present context) [3]. When $Fr > 0.1$, roll waves propagate along the free surface (a similar point of view is presented in Chap. 22). This phenomenon may explain the presence of surges described by most observers for muddy debris flows. Another problem of great interest is the shape of deposit. The longitudinal profile of lobes and levees can be computed using a set of equations similar to (21.9)–(21.10) (a more general set of equations of motion is required to take two-dimensional or three-dimensional spreading into account). For instance in the case of a lobe

stopped over a plane inclined at θ , it can be shown that the longitudinal profile $h(x)$ is given by:

$$\frac{\rho g \sin^2 \theta}{\tau_c \cos \theta} x = -\frac{\rho g \sin \theta}{\tau_c} h - \ln \left(1 - \frac{\rho g \sin \theta}{\tau_c} h \right). \quad (21.12)$$

Equation (21.12) can be used to determine the yield stress in the field. If appropriate, the motion equation set can be cast in a dimensionless form, which yields three dimensionless number. In addition to the Froude number, we introduce a dimensionless shear stress and a generalized Reynolds number [3,34]:

$$G = \frac{\rho g h \sin \theta}{\tau_c}, \quad Re = \frac{\rho \bar{u}^2}{K} \left(\frac{h}{\bar{u}} \right)^n, \quad (21.13)$$

which characterise bulk behaviour for Herschel–Bulkley fluids. These three dimensionless numbers can be used to simulate debris flows with small-scale models.

The Rheological Behaviours of Natural Slurries

On the whole, we can consider as a first approximation that soil–water mixtures involved in debris flows behave as homogeneous fluids. The solid concentration, particle-size distribution and shear rate are the key ingredients in the behaviour of natural suspensions:

- The solid volume concentration ϕ (ratio of solid volume to total volume) usually ranges from 50% to nearly 90%. The upper bound is imposed by geometrical constraints on grains. Indeed, when the solid concentration comes closer to the maximum solid concentration (0.635 for monosized suspensions, much larger for polydisperse suspensions), grain motion is increasingly impeded. Close to the maximum concentration, the material can no longer be sheared without fracturing. The lower bound reflects the minimal amount of particles required for all the particles to be in suspension. If the concentration is too low, the coarsest particles rapidly settle and the mixture can no longer be considered as a homogeneous suspension.
- When the particle-size distribution is great, typically ranging from 0.1 μm to 1 cm, interaction between particles and the surrounding fluid takes various forms [37]. For relatively small shear rates, the finest particles are generally very sensitive to Brownian motion effects or colloidal forces while coarse particles experience frictional or collisional contacts or hydrodynamic forces. As a result, bulk behaviour exhibits either plastic, frictional, or particle-inertia properties.

Microstructural theories and dimensional analysis are useful in outlining the different flow regimes and predicting flow behaviour. We begin the description of natural slurries with suspensions consisting of fine particles, then we examine how bulk behaviour is changed when the coarse-particle fraction is increased (i.e. when the particle size range is widened).

Natural suspensions of fine particles (of diameter d less than $1\ \mu\text{m}$) are usually colloidal suspensions, made-up of weakly-aggregated flocs in water. They generally exhibit viscoplastic behaviour, with sometimes time-dependent properties (thixotropy) when the solid concentration in fine particles ϕ_k is sufficiently high for particles to interact via surface forces (van der Waals attractive forces, electrostatic repulsive forces, etc.). Usually for active clays such as bentonite in pure water, concentrations as low as 0.1% are sufficient to cause the appearance of a yield stress, but for natural clay suspensions, a concentration of a few percent is required. In the opposite case, when the solid fraction is too low, the behaviour is Newtonian. A basic explanation for the existence of yield stress in polydisperse colloidal suspensions is provided by the mean-field theory of Zhou et al. [38]. These authors proposed a model for particles governed by van der Waals attractive forces. The input values of the model were Hamaker's constant A , the coordination number, the mean particle diameter d , and an interparticle separation parameter h_0 , which must be fitted from experimental data. They found that the maximum yield stress can be written as:

$$\tau_k = K \left(\frac{\phi_k}{1 - \phi_k} \right)^c \frac{1}{d^2}, \quad (21.14)$$

where $K = 3.1Ab/(24\pi h_0)$, and b and c are two parameters to be fitted from experimental data. They proposed the following explanation for the variation in yield stress with increasing solid concentration. A weakly flocculated dispersion may be seen as a series of weakly interconnected aggregates (flocs) made up of strongly interacting particles. At low solid concentrations, yielding results from the breakdown of the weak links between flocs. At high solid concentrations, yielding is a consequence of the rupture of interparticle bonds and resistance to the deformation of networks. This means that a critical solid concentration ϕ_{crit} separating the two domains should exist. When $\phi_k < \phi_{\text{crit}}$, structural effects due to weak links between flocs prevails over those due to geometric resistance and the yield stress varies with a solid concentration such as $\tau_k \approx K\phi_k^c/d^2$. This effect is included in (21.14) since it can be derived from (21.14) by taking a series expansion to the chief order at $\phi_k = 0$. When $\phi_k > \phi_{\text{crit}}$, the geometric resistance becomes more pronounced, resulting in a much higher dependence on the solid concentration $\tau_k \approx K\phi_k^{c'}/d^2$, with $c' > c$. Zhou et al. [38] considered that from a microstructural point of view, the geometric resistance enhancement is reflected by the increase in particle contacts. Assuming that the coordination number is given by Rumpf's expression ($C_N = 3.1/(1 - \phi_k)$), they arrived at the conclusion that the yield stress may be scaled as a power function of $\phi_k/(1 - \phi_k)$. The series expansion at $\phi_k = 0$ implies that the exponent must be c . Moreover, their experiments with alumina suspensions showed that the critical solid concentration ranged from 0.26 to 0.44 and depended on the particle diameter. As a typical application of Zhou et al.'s theory, we have reported experimental data obtained with kaolin dispersions on Fig. 21.6. It can be seen that the curve provided by (21.7) fits experimental data over a wide range of solid concentrations.

Various physical explanations for viscoplastic behaviour have been proposed. Potanin et al. developed a phenomenological fractal model to determine bulk

behaviour of weakly aggregated dispersions, assuming that particles form aggregates which in turn are connected to form a network [42,43]. Thus they interpreted bulk yield stress as a consequence of chain break-up due to thermal fluctuations and rupture under compressive force. Another conceptual model inspired from glassy dynamics has been proposed by Sollich and co-workers [44,45]. They showed that the bulk mechanical properties can be related to the internal structure (described in terms of the particle energy distribution). To date such models are able to mimic bulk behaviour over a wide range of flow conditions but cannot specify the effects of particle size, size distribution, or solid concentration on the yield stress of a particulate fluid. Consequently, the flow behaviour of fine colloidal particle suspensions is usually described using the empirical Bingham or Herschel–Bulkley constitutive equation (see Chap. 2), whose rheological parameters τ_k and K are functions of the solid fraction ϕ_k while n is almost independent of the solid concentration ($n = 1$ for a Bingham fluid). The generic simple-shear expression is $\tau = \tau_k(\phi_k) + K(\phi_k)\dot{\gamma}^n$. Other empirical relationships, such as the Casson equation ($\sqrt{\tau} = \sqrt{\tau_k} + \sqrt{K\dot{\gamma}}$), are not usual. Another empirical approximation for simple shear flows of colloidal particles involves considering Krieger and Dougherty’s relationship for computing bulk viscosity η_{eq} (see Chap. 3):

$$\eta_{eq} = \frac{\tau}{\dot{\gamma}} = \eta \left(1 - \frac{\phi}{\phi_m} \right)^{-[\eta]\phi_m}, \tag{21.15}$$

where η is the water viscosity and $[\eta_{eq}] = \lim_{\phi \rightarrow 0} (\eta_{eq} - \eta)/(\eta\phi)$ is called the intrinsic viscosity. To reproduce the viscoplastic behaviour, it is assumed that the maximum solid fraction ranges from a lower value ϕ_0 to an upper bound ϕ_∞ depending on the shear stress [39,40,41].

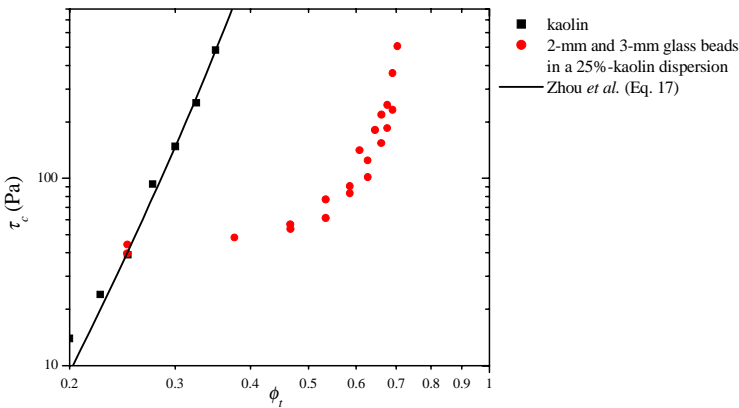


Fig. 21.6. Variation of the yield stress with solid concentration for kaolin–water dispersion and suspensions of glass beads in a kaolin dispersion. On the abscissa axis, ϕ_t denotes the total solid concentration ($\phi_t = \phi_c + \phi_k(1 - \phi_c)$). Adapted from [49]

When the particle size distribution is widened, the coarsest particles can no longer be considered as colloidal. As pointed out by Sengun and Probstein in their investigations of the viscosity of coal slurries [46,47,48], a useful approximation is to consider such mixtures as suspensions of force-free particles in a colloidal dispersion. As it is the interstitial phase, the dispersion resulting from the mixing of fine particles and water imparts most of its rheological properties to the entire suspension (see Chap. 3). Secondly, the coarse fraction is assumed to act independently from the fine fraction and enhance bulk viscosity. Experiments on the viscosity of coal slurries performed by Sengun and Probstein [46,47,48] confirmed the reliability of this concept. A typical example is provided in Fig. 21.6: we added glass beads to a water–kaolin suspension; adding a small amount of beads did not change the bulk stress significantly. Likewise, in their investigations of the behaviour of sand particle suspensions in a natural mud dispersion, Coussot and Piau also found that bulk behaviour was dictated by the fine fraction [16]. The force-free particle assumption is reliable provided the coarse particles are not too heavy (otherwise they settle), that is, they are borne by the surrounding colloidal suspension. This can be expressed in terms of dimensionless numbers by the condition: $N < 1$ where $N = \rho'ga/\tau_k$ denotes the ratio of the buoyant force to the yield stress $\tau_k(\phi_k)$, a is the radius of coarse particles, ρ' is the buoyant density ($\rho' = \phi_c[\rho_c - (\phi_k\rho_k + \rho_0 - \phi_k\rho_0)]$, with ρ_c the coarse-particle density, ρ_k the fine-particle density, and ρ_0 the water density).

When more and more coarse particles are added to a colloidal suspension, coarse particle motion is increasingly impeded and they begin to interact with each other. For instance for solid concentrations in the coarse fraction ϕ_c exceeding 0.35, Sengun and Probstein observed a significant change in bulk behaviour, that they ascribed to non-uniformity in shear rate distribution within the bulk due to squeezing effects between coarse particles [46,47,48]. Likewise, Coussot and Piau's tests [16] together with Ancey and Jorrot's experiments [49] revealed that adding coarse particles to a dispersion induced an increase in the bulk yield stress. When the solid concentration in the coarse fraction approached its maximum value, the yield stress tended towards infinity (see Fig. 21.6). When the coarse particle fraction ϕ_c comes closer to the maximum value, a network of particles in close contact takes place throughout the bulk and stresses resulting from direct contacts between coarse particles prevail compared to colloidal stresses within the dispersion. Thus, the bulk behaviour is chiefly governed by interactions between coarse particles. Two main contact types can arise depending on the suspension composition and flow features: *direct contact* for which the particle surfaces meet (i.e. the distance separating the particle surfaces is equal to or less than the typical height of particle roughness) and *indirect contact* for which there exists a fluid film between particle surfaces. In the former case, contacts between particles are generally frictional (i.e. they can be described using the Coulomb law) [50], giving rise to frictional (possibly collisional) bulk behaviour. Granular debris flows belong to this category. For the latter case, contacts are lubricated and the interstitial fluid still imparts most of its rheological characteristics to the bulk:

- If the interstitial fluid is Newtonian with viscosity η , the (squeezing) lubrication force \mathbf{f} between two particles of radius a separated by a distance εa (with $\varepsilon \ll 1$) is proportional to their relative velocity U : $|\mathbf{f}| = 3\pi\eta a U / (2\varepsilon)$. To evaluate the strength of the squeezing effect, we can define a dimensionless number Γ by dividing the squeezing force by the buoyant force experienced by a test particle. In very concentrated suspensions, a network of particles in direct contact occurs, the gravity force is transmitted through the different layers such that at a depth h , a particle experiences an average “effective” normal stress $\varrho'gh$. In this case, the corresponding dimensionless number is:

$$\Gamma = \frac{9}{4} \frac{a}{\varepsilon} \frac{\eta \dot{\gamma}}{\varrho'gh} . \quad (21.16)$$

Several experiments have shown that Γ is the relevant dimensionless number in the behaviour of concentrated suspensions when particles come in close contact. For instance, Acrivos and co-workers [51] have demonstrated that the viscous resuspension of an initially settled bed of particles is controlled by Γ . Likewise Ancey and Coussot [27] have shown that Γ could scale the flow curves for suspensions of heavy particles within a Newtonian fluid. Figure 21.7 shows such a scaling for a suspension of glass-beads within a Newtonian fluid (water–glycerol solution). A transition in the bulk behaviour can be observed at a critical value Γ ranging from 10^{-3} to 10^{-1} depending on the interstitial fluid viscosity. When $\Gamma \ll 1$, bulk behaviour is typically frictional, namely the shear stress is independent of the shear rate and varies linearly with the normal stress. Conversely when $\Gamma \gg 1$, bulk behaviour is typically Newtonian, namely the shear stress is proportional to the shear rate. Such a transition may explain the amazing behaviour and mobility of lahar-like debris flows.

- For non-Newtonian interstitial fluids, no analytical expression of the squeezing force is available. However, under the condition $N < 1$, it is expected that bulk behaviour is dictated by the interstitial fluid. This explains that, even loaded with a large amount of boulders (giving the impression that the debris is granular), a muddy debris flow behaves as a viscoplastic fluid.

Using microstructural arguments, we have shown that the different types of debris flow behaviour reflect the microstructure properties. Dimensionless groups can also be used to delimit the different flow regimes. The main difficulty in extrapolating these dimensionless numbers to field data is that we have considered truly bimodal suspensions. Natural suspensions are characterised by a continuous gradation in particle size and the cut-off between colloidal and coarse particles, ranging from 4 to 50 μm depending on the authors, is not a fixed value. It results that, in practice, inferring the debris flow type from the material composition is reserved to a limited number of cases, for which the role of different particle-size classes can be determined with sufficient accuracy.

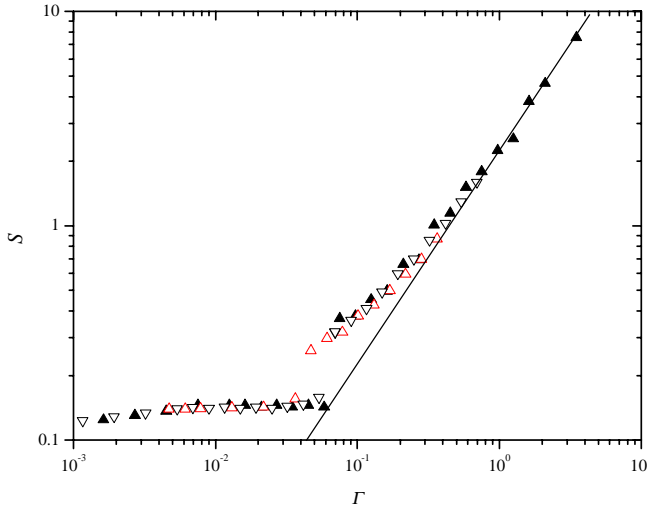


Fig. 21.7. Variation of the dimensionless shear stress $S = \tau/(\rho gh)$ (with h the flow depth) as a function of the dimensionless number Γ . The drawn line has a slope of 1 ($S \propto \Gamma$). Experiments performed with 1-mm glass beads in a water–glycerin solution. Adapted from [27]

References

1. K.M. Scott: ‘Origins, behavior, and sedimentology of lahars and lahars-runout flows in the Toutle-Cowlitz river system’. Report 1447-A (U.S. Geological Survey, 1988)
2. B. Voight: *J. Volcan. Geotherm. Res.* **44**, 349 (1990)
3. P. Coussot: *Mud Flow Rheology and Dynamics* (Balkema, Rotterdam 1997)
4. D. Brunsten, D.B. Prior: *Slope Instability* (John Wiley & Sons, New York 1984)
5. M. Zimmermann, P. Mani, P. Gamma, P. Gsteiger, O. Heiniger, G. Hunziker: *Murganggefahr und Klimaänderung – ein GIS-basierter Ansatz* (VDF, Zürich 1997)
6. P. Coussot, M. Meunier: *Earth Sci. Rev.* **3-4**, 209 (1996)
7. R.M. Iverson: *Rev. Geophys.* **35**, 245 (1997)
8. T. Takahashi: *Ann. Rev. Fluid Mech.* **13**, 57 (1981)
9. V. Koulinski: Étude de la formation d’un lit torrentiel par confrontation d’essais sur modèle réduit et d’observations de terrain. Ph.D. Thesis, University Joseph Fourier, Grenoble (1993)
10. D. Rickenmann: *J. Hydraul. Eng. ASCE* **117**, 1419 (1992)
11. G.M. Smart, M.N.R. Jaeggi: Sedimenttransport in steilen Gerinnen. Mitteilungen 64 (Versuchsanstalt für Wasserbau, Hydrologie und Glaziologie, Zürich 1983)
12. C. Tognacca: Beitrag zur Untersuchung der Entstehungsmechanismen von Murgängen. Ph.D. Thesis, Eidgenössischen Technischen Hochschule Zürich, Zürich (1999)
13. S. Lanzoni: Meccanica di miscugli solido–liquido in regime granulo inerziale. Ph.D. Thesis, University of Padova, Padova (1993)

14. J.J. Major: Experimental studies of deposition of debris flows: process, characteristics of deposits, and effects of pore–fluid pressure. Ph.D. Thesis, University of Washington, Washington (1996)
15. A.M. Johnson, J.R. Rodine: ‘Debris flow’. In: *Slope Instability*, ed. by D. Brundsen, D.B. Prior (John Wiley & Sons, New York 1984) pp. 257–361
16. P. Coussot, J.-M. Piau: *Can. Geotech. J.* **32**, 263 (1995)
17. P. Coussot, D. Laigle, M. Arratano, A. Deganutti, L. Marchi: *J. Hydraul. Eng. ASCE* **124**, 865 (1998)
18. P. Coussot, S. Proust, C. Ancey: *J. Non-Newtonian Fluid Mech.* **66**, 55 (1996)
19. J.J. Major, T.C. Pierson: *Water Resour. Res.* **28**, 841 (1992)
20. C. J. Phillips, T.R.H. Davies: *Geomorphology* **4**, 101 (1991)
21. Z. Wan, Z. Wang: *Hyperconcentrated flow* (Balkema, Rotterdam 1994)
22. P. Coussot: *Les laves torrentielles, connaissances pratiques à l’usage du praticien* (in French) (Cemagref, Antony 1996)
23. T. Takahashi: *Debris flow* (Balkema, Rotterdam 1991)
24. C. Ancey: Rhéologie des écoulements granulaires en cisaillement simple, application aux laves torrentielles granulaires. Ph.D. Thesis, Ecole Centrale de Paris, Paris (1997)
25. C.-L. Chen: *Rev. Eng. Geology* **7**, 13 (1987)
26. J.T. Jenkins, E. Askari: ‘Hydraulic theory for a debris flow supported on a collisional shear layer’. In: *International Workshop on Floods and Inundations related to Large Earth Movements, Trent 1994*, IAHR (IAHR, 1994) pp. 6
27. C. Ancey, P. Coussot: *C. R. Acad. Sci., ser. B* **327**, 515 (1999)
28. D. Rickenmann: *Natural Hazards* **19**, 47 (1999)
29. D. Rickenmann: *Schweizer Ingenieur und Architekt* **48**, 1104 (1996)
30. D. Laigle, P. Coussot: *J. Hydraul. Eng. ASCE* **123**, 617 (1997)
31. C.C. Mei, M. Yuhi: *J. Fluid Mech.* **431**, 135 (2001)
32. B. Hunt: *J. Hydraul. Eng. ASCE* **110**, 1053 (1983)
33. B. Hunt: *J. Hydraul. Eng. ASCE* **120**, 1350 (1994)
34. X. Huang, M.H. Garcia: *J. Fluid Mech.* **374**, 305 (1998)
35. X. Huang, M.H. Garcia: *J. Hydraul. Eng. ASCE* **123**, 986 (1997)
36. J.M. Piau: *J. Rheol.* **40**, 711 (1996)
37. P. Coussot, C. Ancey: *Phys. Rev. E* **59**, 4445 (1999)
38. Z. Zhou, M.J. Solomon, P.J. Scales, D.V. Boger: *J. Rheol.* **43**, 651 (1999)
39. C.R. Wildemuth, M.C. Williams: *Rheol. Acta* **24**, 75 (1985)
40. C.R. Wildemuth, M.C. Williams: *Rheol. Acta* **23**, 627 (1984)
41. S. Mansoutre, P. Colombet, H. Van Damme: *Cement Concrete Res.* **29**, 1441 (1999)
42. A.A. Potanin, R. De Rooi, D. Van den Ende, J. Mellema: *J. Chem. Phys.* **102**, 5845 (1995)
43. A.A. Potanin, W.B. Russel: *Phys. Rev. E* **53**, 3702 (1996)
44. P. Sollich: *Phys. Rev. E* **58**, 738 (1998)
45. P. Sollich, F. Lequeux, P. Hébraud, M.E. Cates: *Phys. Rev. Lett.* **78**, 2020 (1997)
46. M.Z. Sengun, R.F. Probstein: *Rheol. Acta* **28**, 382 (1989)
47. M.Z. Sengun, R.F. Probstein: *Rheol. Acta* **28**, 394 (1989)
48. R.F. Probstein, M.Z. Sengun, T.-C. Tseng: *J. Rheol.* **38**, 811 (1994)
49. C. Ancey, H. Jorrot: *J. Rheol.* **45**, 297 (2001)
50. C. Ancey, P. Coussot, P. Evesque: *J. Rheol.* **43**, 1673 (1999)
51. A. Acrivos, R. Mauri, X. Fan: *Int. J. Multiphase Flow* **19**, 797 (1993)